The threshold photoelectron spectrum of mercury

H Rojas[1], G Dawber[2], N Gulley[2], G C King[2], N Bowring[3], R Ward[4].

[1] Centro de Microscopía Electrónica y Escuela de Física, Facultad de Ciencias, Universidad Central de Venezuela, A.P. 20513. Caracas 1020-A Venezuela

[2] School of Physics and Astronomy, Schuster Laboratory, Manchester University, Manchester M13 9PL, UK.

[3] Faculty of Science & Engineering, John Dalton Building, Chester Street, Manchester, M1 5GD, UK.

[4] School of Computing and Engineering, University of Huddersfield, Queensgate, Huddersfield, HD1 3DH, UK.

Abstract

The threshold photoelectron spectrum of mercury has been recorded over the energy range (10-40 eV) which covers the region from the lowest state of the singly charged ion, $5d^{10}6s$ ($^2S_{1/2}$), to the double charged ionic state, $5d^9(^2D_{3/2})6s(^1D_2)$. Synchrotron radiation has been used in conjunction with the penetrating-field threshold-electron technique to obtain the spectrum with high resolution. The spectrum shows many more features than observed in previous photoemission measurements with many of these assigned to satellite states converging to the double ionisation limit.

PACS numbers:
34.80.Dp Atomic excitation and ionisation
34.10.+x General theories and models of atomic and molecular collisions and interactions (including statistical theories, transition state, stochastic and trajectory models, etc.)

[2] Corresponding Author, e-mail: george.king@manchester.ac.uk

1. Introduction

Since the pioneering work of Beutler and co-workers on the absorption spectra of HgI in the 1930's [1][2][3], there have been numerous studies of mercury from both experimental and theoretical standpoints. In his studies Beutler obtained the absorption spectra of mercury in the vacuum UV region and arranged the observed transitions in Rydberg series. He attributed these series to the inner-shell processes $5d^{10}6s^2(^1S_0) \rightarrow 5d^96s^2(^2D_{3/2,5/2})$ np,nf. Beutler also indicated that the broadening of the observed peaks could be due to the interaction of these discrete states with underlying continua. Extensions of these studies have been carried out by Garten and Connerade [4] over the range 13 – 20 eV, and Mansfield [5] over the range 14 - 33.5 eV. New features were observed that were ascribed to two-electron transitions of the types $5d^{10}6s^2(^1S_0) \rightarrow 5d^96s6pns,np$ and $5d^{10}6s^2(^1S_0) \rightarrow 5d^{10}6pns,nd$. Learner and Morris [6] observed five new autoionising levels belonging to the $5d^96s^26p$, $5d^{10}6p^2$ and $5d^96s^27s$ configurations, and reassigned a number of levels in the HgI spectrum. Martin et al [7][8] carried out intermediate coupling calculations, with configuration interactions on a number of autoionising levels [8], and established the most appropriate designations for these levels. Knowledge of these autoionising levels is important when measuring threshold photoelectron spectra as they may decay into ionic states and so effect their photoionisation cross sections, and hence their observed intensity in the spectrum.

Berkowitz et al [9] reported the valence photoelectron spectrum of mercury. In their work, in addition to the one-electron transitions that produce the "main lines", $5d^{10}(^1S)6s(^2S_{1/2})$ and $5d^96s^2$ $(^2D_{5/2,3/2})$, they observed features corresponding to the formation of excited ionic states $5d^{10}(^1S)6p$ $(^2P_{1/2,3/2})$ states. These excited states of the ion appear in a photoelectron spectrum as 'satellite lines' at higher energies than the "main lines". Being a two-electron process satellite excitation is not allowed in the "single-particle" approximation. The excitation of satellite states is in fact dominated by electron-electron correlations. This is manifested in the irregular behaviour of the series intensities and in the strong mixing of configurations. From a practical point of view, this results in the low cross sections for excitation of satellites whose intensities are typically of the order of a few per cent of the corresponding main line. The interest in satellite states lies in the investigation of their spectroscopy and the dynamics of their formation, and also in comparisons with theoretical predictions. Berkowitz et al presented calculations that indicated Initial State Configuration Interaction (ISCI) was responsible for approximately 80% of the $(^2P_{1/2,\ 3/2})$ intensities observed. They also reported the formation of satellite states that may have the configuration $5d^96p^2$ and/or $5d^96s7s$. Shannon and Codling have measured the partial photoionisation cross section of mercury (15-35 eV) using photoelectron spectroscopy [10]. They observed, in agreement with theoretical calculations by Walker and Waber [11], that the $5d^96s^2$ $(^2D_{5/2}):(^2D_{3/2})$ branching ratio deviates from the statistical branching ratio of 1:1.5, as a function of the photon energy. In addition to

this, Süzer et al have studied mercury using photoelectron spectroscopy [12] and observed satellite peaks corresponding to the configurations $5d^{10}6p$ ($^2P_{1/2,\ 3/2}$). They attributed these states to ISCI, confirming the results of Berkowitz et al [9]. More recently, Eland and Feifel [13] have used a time-of-flight photoelectron-photoelectron coincidence technique to report photoelectron pair distributions from single photon double ionisation of Mercury at 40.8 and 48.4eV. The authors also recorded single ionisation photoelectron spectra, detailing new satellite structure below the double ionisation limit, and undertook relativistic calculations to update the work of Berkowitz et al [9]. They also emphasise that substantial mixing of the excited configuration $5d^{10}6p^2$ in the ground state of the Hg atom could be responsible for weak configuration interaction satellites linked to the formation of the $5d^{10}6p$ configuration of Hg+. Toffoli et al. [14] have undertaken a relativistic time-dependent density function theory approach and Zubek et al. [15] have studied photoionisation differential cross sections for the $5d^96s^2\ ^2D_{5/2}$ ionic state of mercury (15-17 eV), together with determining the variation of the asymmetry β-parameter as a function of photon energy across this energy range. Finally, Baig has undertaken high resolution measurements and multichannel quantum defect theory analysis of autoionising resonances in mercury [16].

As far as we are aware the threshold photoelectron spectrum of mercury has not been reported previously. Threshold photoelectron spectroscopy (TPES) has contributed significantly to our knowledge of the electronic structure of atomic and molecular ion systems [17], with the photoionization of an atom or molecule just above its threshold bringing a new perspective of ionization as compared with conventional photoelectron spectroscopy (PES). With low signal to noise ratios, very high-resolution spectra (~1 meV) are often obtained, with spectral resolution governed essentially by the bandwidth of the photon source. In addition, the threshold spectra are essentially free from Doppler effects.

2. Apparatus and experimental procedures

The threshold photoelectron spectra were obtained using the Synchrotron Radiation Source (SRS) of Daresbury Laboratory, UK. Details of the experimental arrangement have been given previously [18] [19]. Synchrotron radiation emanating from the source was dispersed by the 5-m normal incidence McPherson monochromator on beamline 3.2. The dispersed light was transported to the interaction region through a 1 mm bore by a 35 cm long glass capillary tube. The output end of the capillary tube was approximately 20 mm from the photon/atomic beam interaction region. The mercury beam emanated from a capillary tube of internal bore 1.6 mm and length 20 mm that was connected to a resistively heated oven. The oven comprised of a reservoir containing liquid mercury and an arm connecting it to the capillary tube as shown in Figure 1. The reservoir, connecting arm and oven orifice were separately heated using twin-core, non-inductive Thermocoax heating elements. To avoid clogging, the temperature of the needle was kept higher than any other part of the oven. A total power of 15W was delivered to the heating elements from a constant current power supply. This maintained a reservoir temperature of 70°C and a target pressure in the interaction region of approximately 10^{-1} Pa. The oven was loaded with 20 cm^3 of mercury, supplied by Goodfellow Metals Ltd and this was sufficient for about 1000 hours of continuous operation. The oven was electrically isolated, so it could be independently biased with respect to the interaction region to counteract the effects of surface patch fields. It was mounted on an adjustable base that allowed the oven orifice to be accurately positioned with respect to the interaction region, defined by the intersection of the photon beam and the optical axis of the photoelectron spectrometer (a schematic of which is shown in Figure 2). The oven also contained a side inlet for an additional gas, usually argon, to be introduced through the orifice into the scattering region. This facilitated tuning of the spectrometer and energy calibration of the incident photon energy. A commercial nitrogen cold trap was placed between the chamber and the turbo molecular pump to prevent mercury vapour from reaching the rest of the pumping system. Additional pumping action was obtained from a large cooled copper plate. This plate was cooled via a liquid nitrogen cold finger and was placed opposite to the mercury oven output to collect any residual mercury vapour.

Zero-energy (threshold) electrons produced in the photoionization of mercury were collected and selected using the penetrating field technique [20]. Here a weak electrostatic field penetrates into the interaction region. This field collects the threshold electrons over a 4π solid angle with almost 100% efficiency but discriminates against higher energy photoelectrons. 95% of the detected electrons have energies below 3meV, as determined from the threshold spectrum of the argon-ion doublet lines at 15.759eV ($^2P_{3/2}$) and 15.937eV ($^2P_{1/2}$). Energy calibration of the threshold photoelectron spectra in mercury was obtained by comparing the observed positions of the main line and satellite states of mercury observed in this work against their spectroscopically known values [21]. These states extend over a range

of approximately 10eV and so also provide a valuable check on the linearity of the photon energy scale. This calibration was checked by observing the positions of the Ar+ 3s($^2P_{3/2,1/2}$) states at 15.759 and 15.937eV respectively and the Ar+ 3s ($^2S_{1/2}$) state at 29.237eV. The agreement was within a few meV. The spectra were normalised to the incident photon flux using an aluminium photodiode placed downstream of the interaction region.

Constant Ionic State (CIS) spectra [22] were collected alongside the threshold photoelectron spectra, providing a further calibration process. An example of these spectra, which will be published separately, is shown in Figure 3. In the current work these CIS spectra provided further information on resonance series and their decay. For example the highly asymmetric nature of the profiles in Figure 3 suggest significant interference between direct and indirect decay channels.

3. Results and discussion

3.1 Threshold photoelectron spectrum of the lower lying ionic states of mercury (10.4 to 16.8 eV)

The threshold photoelectron spectrum of mercury in the region of the lower lying ionic states is shown in Figure 4. The photon bandpass was 0.5A corresponding to 9meV at 15eV, and the step size was 2meV. As indicated, three of the observed features correspond to the $5d^{10}6s$ ($^2S_{1/2}$) and $5d^96s^2$ ($^2D_{5/2,3/2}$) ionic states (main lines) of outer-shell ionisation. The last two of these features agree very well with the 14.840eV $^2D_{5/2}$ and 16.705eV $^2D_{3/2}$ ionisation thresholds of Zubek et al. [15]. The relative intensities for the ($^2S_{1/2}$), ($^2D_{5/2}$) and ($^2D_{3/2}$) peaks are 2:1:2.4. The ratio for the ($^2D_{5/2}$), ($^2D_{3/2}$) peaks deviates considerably from the expected statistical ratio of 1.5:1, and is in disagreement with the partial cross section measurements of Shannon and Codling [10]. In that work the intensity of the ($^2D_{5/2}$) peak was always greater than that of the ($^2D_{3/2}$) peak and an extrapolation to threshold ionisation gave a ratio of the order of 2.6:1. The relative increases of the ($^2S_{1/2}$), ($^2D_{5/2}$) cross sections at threshold are attributed to the decay of auto-ionising states into these ionic states. The shapes of the three main line features are consistent with the shape of the transmission function of the threshold spectrometer. This shape was measured independently by observing the $^2P_{3/2,1/2}$ states of Ar+, and is well represented by an asymmetric Gaussian with a sharp rise and a more gradual fall. In addition, the ($^2S_{1/2}$) peak shows a small increase just before the rising edge as is also observed for the $^2P_{3/2}$ state of Ar+. The nature of this increase is not certain but it may originate from the ionisation of high-Rydberg states converging on the ($^2S_{1/2}$) limit.

The additional, prominent peak lying 32meV above the $5d^96s^2(^2D_{5/2})$ threshold corresponds to the resonance $[5d^96s^2(^2D_{3/2})]7p$. It is observed here because of the high-energy tail in the transmission function of the threshold spectrometer. This tail is only slight as can be judged from the shape of the ($^2S_{1/2}$) peak. Indeed at an energy of 32meV above threshold the transmission function has fallen to 0.02% of its maximum value. By acquiring CIS spectra

alongside the TPES spectra, as discussed above, we are able to identify and separate these ionic and neutral resonance features.

3.2. Threshold photoelectron spectrum of satellite states of mercury (16.5 to 37.5 eV)

Satellites correspond to excited states of the singly charged ion and form series that converge to doubly charged states of the ion. The doubly charged states of Hg^{++} relevant to the present work are $5d^{10}(^1S_0)$, $5d^9(^2D_{5/2})6s(^3D_{3,2})$ and $5d^9(^2D_{3/2})6s(^3D_1,^1D_2)$. These have energies between 29 and 37eV. The threshold photoelectron spectrum of mercury in the energy region leading up to these doubly charged ion states is shown in Figure 5 to Figure 9. This spectrum is the result of 10 independent measurements covering the energy range 16.5 to 37.5eV with a typical step size of 3meV. The photon bandpass was fixed at 0.28A, resulting in a spectral resolution that varied smoothly from 6meV at 16eV to 31meV at 37.5eV. The majority of the observed features correspond to the formation of singly charged satellite states. The binding energies of all the observed features are summarised in Table 1 to Table 27. In the case of broad, unresolved features the peak energy value is given. The uncertainty in the measured energies is estimated to be ±5meV. It has been attempted, where possible, to arrange the tables in terms of Rydberg series of satellite states.

3.2.1. The $5d^{10}$ (^1S) nl series of satellite states

The $5d^{10}(^1S_0)$ state of Hg^{++} occurs at an energy of 29.19eV above the neutral ground state and most of the observed features below this energy are expected to be satellite states converging to this limit. The present assignment of the features is mainly based on the assignments proposed by Moore [21]. Six series with configurations $5d^{10}(^1S_0)$ nl have been identified. The measured energies are presented in Table 1 to Table 6, where they are compared to the values of Moore. In general, good agreement is found between the two sets of energies. The assigned $5d^{10}(^1S_0)$ nl series in the region below the $5d^{10}(^1S_0)$ state of Hg^{++} are shown in Figure 10. Due to the relatively high intensities of the peaks near this threshold, no attempt has been made to extend any of the $5d^{10}(^1S_0)$ nl series beyond the reported n. Instead, the observed features near the threshold are considered to be due to satellite states converging to higher lying doubly charged states.

3.2.2. The $5d^9$ 6s np series of satellite states

The $5d^9$6s6p configuration of Hg^+ can lead to 23 possible states. The energies and tentative assignments (in j-j coupling) of 19 of these states have been reported by Moore [21]. Each of these states is a member of a Rydberg series that converges to one of the four doubly charged states $^3D_3$, $^3D_2$, $^3D_1$ or $^1D_2$. Up to now there has been no report of higher members of these satellite series, above n = 6, and of the specific limits associated with each of them. Here, a Rydberg formula for the possible $^3D_3$, $^3D_2$, $^3D_1$ or $^1D_2$ doubly charged cores has been used to extend the Rydberg series to higher n values and to determine their convergence limit. The quantum defect used for each series was obtained from the n = 6 member, using the energy

positions reported by Moore, and has been assumed to be constant along the series. The selection of the series limit has been made taking into account the configuration of the core. In the case where there exists more than one state with the same core and total angular momentum J, the convergence limit was determined by fitting the calculated series to the observed energies using a linear regression routine and assigning the series in accordance with the "best" fit. Extensions to 18 of the series reported by Moore are presented in Table 7 to Table 24. Near the convergence limits some of the observed series overlap making it difficult to assign them to only one configuration. This is particularly the case in the high energy region where the photon resolution is less good. In general, good agreement is found between the calculated energies and measured energies. From the observations, the quantum defect for all of the satellite Rydberg series is estimated to be 3.9 ± 0.1. Although additional states with higher values of n have been identified using the calculated energies, the relative intensities within a series bears no relationship to the expected variation of $(n^*)^{-3}$. This is likely to be due to the presence of doubly-excited neutral resonance states in this region that decay into the satellite states with the emission of an electron that falls within the transmission function of the analyser. It should be noted that the high sensitivity of the present technique does allow the detection of satellite features that may not have been previously observed in photoelectron studies. Three of the observed peaks, at 30.550, 33.090 and 30.957eV correspond well with those measured by Price and Eland [23] and for which no assignment had previously been given.

3.2.3. **Other features observed in the threshold photoelectron spectrum**

Other features observed in the threshold photoelectron spectrum of Figure 4 to Figure 9 are listed in Table 25 to Table 27. Some of the features seem to show excellent agreement with those observed experimentally and assigned as $5d^96p^2$ by both Eland and Feifel [13] and Berkowitz et al [9]. The assignment of the observed peaks to this configuration by Berkowitz et al [9] was the result of relativistic calculations using Initial State Configuration Interaction in which the $5d^96p^2$ nl ($^1S_0$) and $5d^96s7s$ nl ($^1S_0$) configurations were included. Berkowitz et al noted that the absolute energies of the calculated states is only accurate to within approximately 1eV, but their relative separations are much more reliable. Eland and Feifel [13] also used this approach when they identified $5d^96p^2$ peaks. The values listed in Table 25 to Table 27 are the corrected ones, obtained after shifting the calculated energies by a constant amount to fit the observed peaks [9].

From their results, Berkowitz et al noted that both the ISCI and shake-up mechanisms, responsible for the formation of the $5d^96p^2$ and $5d^96s7s$ states respectively, produce comparable contributions to the intensity of the satellites observed. From the computed intensity ratio between the $5d^96p^2$ and $5d^96s7s$ states of ~1:1.4, they were able to conclude that both final states may be formed. Following the results of Berkowitz et al, the observed features in the present TPES spectrum have been assigned to states with configuration $5d^96p^2$.

However they could also be assigned as $5d^9 6s7s$ or a combination of $5d^9 6p^2$ and $5d^9 6s7s$ states. Taking into account isoelectronic data from the neighbouring atom AuI, $5d^9 6s7s$ states are expected to lie between the $5d^{10}(^1S)8s$ and $5d^{10}(^1S)10d$ states. As a result, the most intense features in this region (designated 47 and 51) have been tentatively assigned to the $5d^9 6s7s$ configuration. Eland and Feifel [13] on the other hand have used the relative separation, as discussed above, to identify two $5d^9 6p^2$ pairings, the $5d^9_{5/2} 6p^2(^3P_0)$ state at 23.64eV and $5d^9_{3/2} 6p^2(^3P_0)$ state at 25.60eV, and a higher pairing of $5d^9_{5/2} 6p^2(^1S_0)$ and $5d^9_{3/2} 6p^2(^1S_0)$ states at 27.87eV and 29.78eV respectively. Whilst there is disagreement regarding the lower pairing, the higher pairing agree well with the current work as do many of their measurements of autoionising states between 29eV and 36eV.

Features indicated according to the notation of Moore [21] as, Y, C, 16^0, $20_{7/2}$, $4D^3$, $4D^3_{1/2}$ and $a_{5/2}$ have also been identified. Extensions of the series have not been carried out since no clear indication of their configuration is given. Other features in the spectrum have been attributed to doubly excited neutral states that decay to the neighbouring satellite states and appear in the spectrum because of the finite transmission of the analyser for non-threshold electrons. The assignment of these states follows that of Mansfield [5]. A lack of theoretical studies in this area means the interpretation of the features in the spectrum is as yet incomplete.

4. Conclusions

We have performed a high-resolution threshold photoelectron spectroscopic study of mercury covering the entire ionization region from the lowest state of the singly charged ion, $5d^{10}6s$ ($^2S_{1/2}$), to the double charged ionic state, $5d^9(^2D_{3/2})6s(^1D_2)$. Twenty nine new features have been observed and assignments made based on their possible configurations and their calculated energies using a Rydberg formula. The intensity ratios between the observed threshold peaks for Hg^+ $^2S_{1/2}$, $^2D_{5/2}$ and $^2D_{3/2}$ differ significantly from the expected statistical values and contradict the extrapolated partial cross section values obtained by Shannon and Codling [10]. The increased partial cross section of the Hg^+ $^2S_{1/2}$ and $^2D_{3/2}$ states at threshold is attributed to the decay of the autoionising neutral states into these continua, with resonance structure found near threshold for these ionic states.

In studying the formation of satellite states Hg^{+*}, over 200 features have been observed in the threshold photoelectron spectrum in the region between the threshold of the third ionic state $5d^9 6s^2$ ($^2D_{3/2}$) and 37.25eV, with almost all attributable to the formation of singly charged satellite states. Extensions to the satellite series for $5d^9 6snp$ have been made using a Rydberg formula for the different doubly charged cores ($5d^9 6s(^3D_{Jc})$). A constant quantum defect, obtained from the energy values reported by Moore [21] has been used. From this the convergence limits of the observed series have been determined. Features indicated according to the notation of Moore [21] as, Y, C, 16^0, $20_{7/2}$, $4D^3$, $4D^3_{1/2}$ and $a_{5/2}$ have been identified in the current work and previously unassigned features agree well with the results of Berkowitz

et al [9] and Eland and Feifel [13], and have been assigned to states with configuration $5d^9 6p^2$.

Acknowledgments

The authors would like to thank the CLRC Daresbury Laboratory for providing beamtime and facilities for carrying out this study.

Tables

Energy (eV)	n	J	Spectro*	I	Code
22.307	7	1/2	22.305	613	24
25.492	8	1/2	25.492	107	46
28.042	11	1/2	28.033	8	71

* Moore (1949)

Table 1 - Measured energies for series $5d^{10}(^1S)ns(^2S)$.

Energy (eV)	n	J	Spectro*	I	Code
16.820	6	1/2	16.821	371	2
17.950	6	3/2	17.952	281	3
23.866	7	1/2	23.865	298	39
24.326	7	3/2	24.321	271	45
27.230	9	1/2	27.234	41	59
27.820§	10	1/2	27.812	252	69§
27.845§	10	3/2	27.838	83	70§

* Moore (1949)
§ More than one configuration

Table 2 - Measured energies for series $5d^{10}(^1S)np(^2P^o)$.

Energy (eV)	n	J	Spectro*	I	Code
23.452	6	3/2	23.454	341	34
23.522	6	5/2	23.524	913	36
25.986§	7	3/2	25.976	41	52§
	7	5/2	26.008		
27.762	9	5/2	27.758	19	68
28.123	10	3/2	28.126	17	74
28.375	11	3/2	28.373	33	78
	11	5/2	28.376		
28.827§	15	3/2	28.826	26	94§
	15	5/2			

* Moore (1949)
§ More than one configuration

Table 3 - Measured energies for series $5d^{10}(^1S)nd(^2D)$.

Energy (eV)	n	J	Spectro*	I	Code
25.715	5	7/2	25.707	27	49
25.740	5	5/2	25.739	32	50
26.993	6(?)	5/2	26.971	9	53
27.643	7	7/2	27.646	61	63
27.650#	7	5/2	27.649	19	64#
28.063	8	7/2	28.060	13	72
	8	5/2	28.060		
28.325§	9	5/2	28.328	16	76§
		7/2	28.328		

* Moore (1949)
§ More than one configuration
# Peak value, possibly more than one state

Table 4 - Measured energies for series $5d^{10}(^1S)nf(^2F^o)$.

Energy (eV)	n	J	Spectro*	I	Code
27.030	5	7/2	27.009	44	56
	5	9/2			
27.672	6	7/2	27.677	102	65
	6	9/2			
28.089	7	7/2	28.080	37	73
	7	9/2			
28.338§	8	7/2	28.342	122	77§
	8	9/2			
28.518§	9	7/2	28.522	72	84§
	9	9/2	28.522		
28.646	10	7/2	28.649	134	87
	10	9/2			
28.738§	11	7/2	28.744	86	90§
	11	9/2			

* Moore (1949)
§ More than one configuration

Table 5 - Measured energies for series $5d^{10}(^1S)ng(^2G)$.

Energy (eV)	n	J	Spectro*	I	Code
28.532#	9	9/2	28.522	72	84§
	9	11/2			
28.659#	10	9/2	28.649	134	87
	10	11/2			

* Moore (1949)
§ More than one configuration
# Peak value, possibly more than one state

Table 6 - Measured energies for series $5d^{10}(^1S)nh(^2H^o)$.

Energy (eV)	n	Calculated value[a]	I	Code
20.325	6	20.320*	250	5
28.217	7	28.290	84	75
31.061	8	31.035	49	144
32.302	9	32.294	15	170
32.970	10	32.975	44	183

* Moore (1949)
[a] Calculated using Rydberg formula with quantum defect = 4.042

Table 7 – Extension of series $5d^9_{5/2}6s_{1/2}np_{1/2}$ (J=5/2) converging to $^3D_3$ limit.

Energy (eV)	n	Calculated value[a]	I	Code
20.879	6	20.879*	176	7
28.437	7	28.454	55	81
31.099	8	31.104	94	146
33.010#	10	32.995	158	184
33.397#	11	33.396	18	188

* Moore (1949)
[a] Calculated using Rydberg formula with quantum defect = 4.002
Peak value, possibly more than one state

Table 8 – Extension of series $5d^9_{5/2}6s_{1/2}np_{1/2}$ (J=7/2) converging to $^3D_3$ limit.

Energy (eV)	n	Calculated value[a]	I	Code
20.953	6	20.956*	167	12
28.738	7	28.755	86	90
31.458#	8	31.458	40	154
32.705#	9	32.703	57	178

* Moore (1949)
[a] Calculated using Rydberg formula with quantum defect = 4.024
Peak value, possibly more than one state

Table 9 – Extension of series $5d^9_{5/2}6s_{1/2}np_{1/2}$ (J=5/2) converging to $^3D_2$ limit.

Energy (eV)	n	Calculated value[a]	I	Code
21.121	6	21.123*	517	15
28.801	7	28.804	34	92
32.705#	9	32.714	57	178

* Moore (1949)
[a] Calculated using Rydberg formula with quantum defect = 4.013
Peak value, possibly more than one state

Table 10 – Extension of series $5d^9_{5/2}6s_{1/2}np_{1/2}$ (J=3/2) converging to $^3D_2$ limit.

Energy (eV)	n	Calculated value[a]	I	Code
-	6	21.915*	-	-
28.768	7	28.767	30	91
33.010#	10	33.035	158	184

* Moore (1949)
[a] Calculated using Rydberg formula with quantum defect = 3.921
Peak value, possibly more than one state

Table 11 – Extension of series $5d^9_{5/2}6s_{1/2}np_{3/2}$ (J=9/2) converging to $^3D_3$ limit.

Energy (eV)	n	Calculated value[a]	I	Code
22.103	6	22.104*	239	19
28.827	7	28.825	29	94
31.264	8	31.262	55	150
32.409#	9	32.411	8	171
33.010#	10	33.043	158	184
33.672#	12	33.677	27	191
33.854	13	33.849	15	193
33.981#	14	33.973	10	194

* Moore (1949)
[a] Calculated using Rydberg formula with quantum defect = 3.906
Peak value, possibly more than one state

Table 12 – Extension of series $5d^9{}_{5/2}6s_{1/2}np_{3/2}$ (J=3/2) converging to $^3D_3$ limit.

Energy (eV)	n	Calculated value[a]	I	Code
22.241	6	22.104*	239	19
29.151#	7	29.140	20	105
31.617#	8	31.621	64	158
32.787	9	32.787	11	179
33.813#	11	33.814	20	192

* Moore (1949)
[a] Calculated using Rydberg formula with quantum defect = 3.927
Peak value, possibly more than one state

Table 13 – Extension of series $5d^9{}_{5/2}6s_{1/2}np_{3/2}$ (J=7/2) converging to $^3D_2$ limit.

Energy (eV)	n	Calculated value[a]	I	Code
22.257	6	22.254*	272	23
28.869	7	28.871	182	95
31.264#	8	31.282	55	150

* Moore (1949)
[a] Calculated using Rydberg formula with quantum defect = 3.893
Peak value, possibly more than one state

Table 14 – Extension of series $5d^9{}_{5/2}6s_{1/2}np_{3/2}$ (J=5/2) converging to $^3D_3$ limit.

Energy (eV)	n	Calculated value[a]	I	Code
22.474	6	22.476*	783	28
29.266#	7	29.213	59	106
31.649#	8	31.652	18	159
32.800	9	32.803	52	180
33.460#	10	33.435	12	189
33.813#	11	33.819	20	192
34.089#	12	34.070	15	195

* Moore (1949)
[a] Calculated using Rydberg formula with quantum defect = 3.893
Peak value, possibly more than one state

Table 15 – Extension of series $5d^9_{5/2}6s_{1/2}np_{3/2}$ (J=5/2) converging to $^3D_2$ limit.

Energy (eV)	n	Calculated value[a]	I	Code
22.939	6	22.943*	603	29
30.426	7	30.423	232	130
34.266#	9	34.253	20	196

* Moore (1949)
[a] Calculated using Rydberg formula with quantum defect = 3.992
Peak value, possibly more than one state

Table 16 – Extension of series $5d^9_{3/2}6s_{1/2}np_{1/2}$ (J=3/2) converging to $^3D_1$ limit.

Energy (eV)	n	Calculated value[a]	I	Code
23.228	6	23.231*	1449	30
34.612#	9	34.596	220	201

* Moore (1949)
[a] Calculated using Rydberg formula with quantum defect = 3.995
Peak value, possibly more than one state

Table 17 – Extension of series $5d^9_{3/2}6s_{1/2}np_{1/2}$ (J=3/2) converging to $^1D_2$ limit.

Energy (eV)	n	Calculated value[a]	I	Code
-	6	23.656*	-	-
30.875#	7	30.869	51	139
33.460#	8	33.430	12	189
35.682#	11	35.669	29	203
35.928#	12	35.926	19	204

* Moore (1949)
[a] Calculated using Rydberg formula with quantum defect = 3.962
Peak value, possibly more than one state

Table 18 – Extension of series $5d^9{}_{3/2}6s_{1/2}np_{3/2}$ (J=1/2) converging to $^1D_2$ limit.

Energy (eV)	n	Calculated value[a]	I	Code
23.313	6	23.316*	1469	32
30.550♦	7	30.534	162	133
33.090♦	8	33.096	100	185

* Moore (1949)
[a] Calculated using Rydberg formula with quantum defect = 3.964
Peak value, possibly more than one state
♦ Price and Eland (1990) (30.5 ± 0.1 eV, 33.1 ± 0.1 eV)

Table 19 – Extension of series $5d^9{}_{3/2}6s_{1/2}np_{1/2}$ (J=1/2) converging to $^3D_1$ limit.

Energy (eV)	n	Calculated value[a]	I	Code
23.341#	6	23.337*	68	33
30.771#	7	30.774	98	137
34.612#	9	34.603	220	201

* Moore (1949)
[a] Calculated using Rydberg formula with quantum defect = 3.987
Peak value, possibly more than one state

Table 20 – Extension of series $5d^9{}_{3/2}6s_{1/2}np_{1/2}$ (J=5/2) converging to $^1D_2$ limit.

Energy (eV)	n	Calculated value[a]	I	Code
-	6	23.617*	-	-
30.628	7	30.626	9	135
33.153	8	33.135	17	186
34.365	9	34.310	43	197

* Moore (1949)
[a] Calculated using Rydberg formula with quantum defect = 3.940
Peak value, possibly more than one state

Table 21 – Extension of series $5d^9{}_{3/2}6s_{1/2}np_{1/2}$ (J=1/2) converging to $^3D_1$ limit.

Energy (eV)	n	Calculated value[a]	I	Code
24.226	6	24.222*	218	43
31.042§	7	31.061	49	144
33.504	8	33.519	7	190
35.682#	11	35.683	29	203

* Moore (1949)
[a] Calculated using Rydberg formula with quantum defect = 3.918
§ More than one configuration
# Peak value, possibly more than one state

Table 22 – Extension of series $5d^9{}_{3/2}6s_{1/2}np_{3/2}$ (J=7/2) converging to $^1D_2$ limit.

Energy (eV)	n	Calculated value[a]	I	Code
23.981	6	23.976*	634	41
30.957♦	7	30.967	37	140
33.460#	8	33.471	12	189

* Moore (1949)
[a] Calculated using Rydberg formula with quantum defect = 3.938
Peak value, possibly more than one state
♦ Price and Eland (1990) (30.9 ± 0.1 eV)

Table 23 – Extension of series $5d^9{}_{3/2}6s_{1/2}np_{3/2}$ (J=3/2) converging to $^1D_2$ limit.

The threshold photoelectron spectrum in mercury

Energy (eV)	n	Calculated value[a]	I	Code
23.981	6	24.151*	247	42
30.785	7	30.790	114	138
33.214	8	33.206	33	187
34.365§	9	34.347	43	196

* Moore (1949)
[a] Calculated using Rydberg formula with quantum defect = 3.896
§ More than one configuration

Table 24 – Extension of series $5d^9_{3/2}6s_{1/2}np_{3/2}$ (J=3/2) converging to $^3D_1$ limit.

Energy (eV)	Previous Energies (eV)	Tentative Assignment	I	Code
16.706	16.706*	$5d^96s^2(^2D_{3/2})$	12962	1
17.966#			72	4
20.346#			31	6
20.887#			78	8
20.896			88	9
20.903#	20.906*	$5d^96s6p(11d)$	118	10
20.911#			80	11
20.976			46	13
21.009	21.013□	$5d^9_{5/2}6s_{1/2}6p_{1/2}14d$ (J=3/2)	16	14
21.136			194	16
21.139#			60	17
21.144			183	18
22.108			156	20
22.130			77	21
22.334#	22.332□	$5d^9_{3/2}6s_{1/2}6p_{1/2}7d$ (J=3/2)	269	25
22.366	22.363*	$5d^9_{5/2}6s_{1/2}6p_{3/2}$ (J=1/2)	1270	26
22.382	22.387□	$5d^9_{3/2}6s_{1/2}6p_{3/2}6d$ (J=3/2)	151	27
23.234			313	31
23.485			41	35

23.590	23.591*	Y	1387	37
	23.7♦			
	23.64♠	$5d^9(5/2)6p^2(^3P_0)$		
23.607	23.607*	$16^{O\,*}$(J=7/2)	483	38
23.953	23.949*	$20_{7/2}{}^{*}$(J=7/2)	337	40
24.231			65	44
25.532		$5d^96s7s$ (?)	572	47
	25.60♠	$5d^9(3/2)6p^2(^3P_0)$		
25.553#	25.559*	C^* (J=5/2)	186	48
25.892	25.8♦	$5d^96s7s$ (?)	202	51
26.639			84	53
26.892	26.893*	$4D^3$ (J=7/2)	11	54
27.044			35	57
27.171#			14	58
27.247			40	60
27.293			20	61
27.402	27.50●	$5d^96p^2$	484	62
27.699			70	66
27.719			16	67
27.762	27.75●	$5d^96p^2$	19	68
27.845	27.9♦	$5d^96p^2$	83	70
	27.80■			
	27.87♠	$5d^9(5/2)6p^2(^1S_0)$		
28.217	28.26■	$5d^96p^2$	84	75
28.325	28.32●	$5d^96p^2$	16	76

♦ Price and Eland (1990) (± 0.1 eV)

* Moore (1949)
● Berkowitz et al (1974) (Corrected)
■ Berkowitz et al (1974) (Measured, ± 0.05 eV)
Peak value, possibly more than one state
□ Mansfield (1973)
♠ Eland and Feifel (2004)

Table 25 – Measured energies of other features in the TPES spectrum of mercury (16.71-28.32eV)

Energy (eV)	Previous Energies (eV)	Tentative Assignment	I	Code
28.338	28.33●	$5d^9 6p^2$	122	77
28.387			43	79
28.406	28.405*	$4D^3_{½}{}^*$(J=1/2)	67	80
28.440			15	82
28.472			9	83
28.572#			15	85
28.622	28.620*	$a_{5/2}{}^*$ (J=5/2)	214	86
28.669#			61	88
28.721			106	89
28.813			117	93
28.894			43	96
28.919			98	97
28.957			76	98
28.978			135	99
29.018			47	100
29.069			15	101
29.080			50	102
29.117#			16	103
29.131			11	104
29.279			41	107
29.346	29.33●	$5d^9 6p^2$	60	108
29.383#			54	109
29.407			78	110

29.455#			102	111
29.527#	29.58●	$5d^9 6p^2$	83	112
29.582#			31	113
29.645			24	114
29.680	29.70♦		120	115
29.708	29.70♦		75	116
29.747	29.73■	$5d^9 6p^2$	267	117
	29.73♠			
	29.75●			
	29.77●			
29.782		$5d^9 6p^2$	41	118
	29.78♠	$5d^9(3/2)6p^2(^1S_0)$		
29.832			25	119
29.964			63	120
30.005			61	121
30.033			59	122
30.056			39	123
30.105#	30.10●	$5d^9 6p^2$	49	124
30.118			91	125
30.177			110	126
30.212			55	127
30.262			9	128
30.405#	30.39♠		39	129
30.477#			60	131

♦ Price and Eland (1990) (± 0.1 eV)
* Moore (1949)
● Berkowitz et al (1974) (Corrected)
■ Berkowitz et al (1974) (Measured, ± 0.05 eV)
Peak value, possibly more than one state
□ Mansfield (1973)
♠ Eland and Feifel (2004)

Table 26 - Measured energies of other features in the TPES spectrum of mercury (28.33 - 30.48eV)

The threshold photoelectron spectrum in mercury

Energy (eV)	Previous Energies (eV)	Tentative Assignment	I	Code
30.524	30.53♠		30	132
30.565			36	134
30.683			55	136
30.987	30.9♦		86	141
30.992#			30	142
31.015			53	143
31.079			70	145
31.117			59	147
31.173#			23	148
31.184			19	149
31.358#			34	151
31.370			52	152
31.408			32	153
31.543#			93	155
31.551	31.55●	$5d^9 6p^2$	126	156
31.580			33	157
31.770#			17	160
31.908			26	161
31.933			17	162
31.975			73	163
31.984			15	164
31.993			33	165
32.062	32.1♦		137	166
	32.05♠			
32.088			27	167
32.174#			16	168
32.240#			19	169

32.526#		10	172
32.537		30	173
32.560		25	174
32.568		13	175
32.634#		26	176
32.687#		145	177
32.887#		20	181
32.940#	33.06♠	29	182
34.415		41	198
34.466#	34.45♠	53	199
34.551#	34.58♠	72	200
	34.89♠		
35.184#		33	202
35.973#	35.64♠	29	205
	35.85♠		
	35.93♠		

♦ Price and Eland (1990) (± 0.1 eV)
* Moore (1949)
● Berkowitz et al (1974) (Corrected)
■ Berkowitz et al (1974) (Measured, ± 0.05 eV)
Peak value, possibly more than one state
□ Mansfield (1973)
♠ Eland and Feifel (2004)

Table 27 - Measured energies of other features in the TPES spectrum of mercury (30.52 - 35.98 eV)

Figures

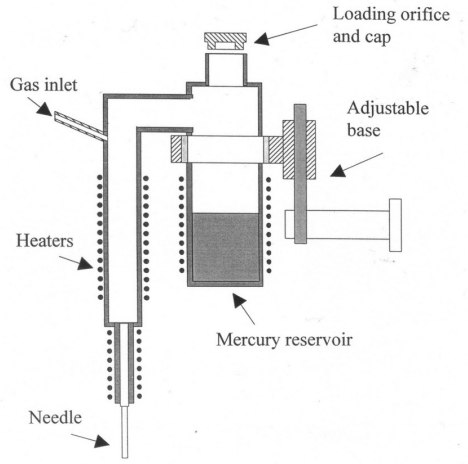

Figure 1 - Schematic of Mercury Vapour Source

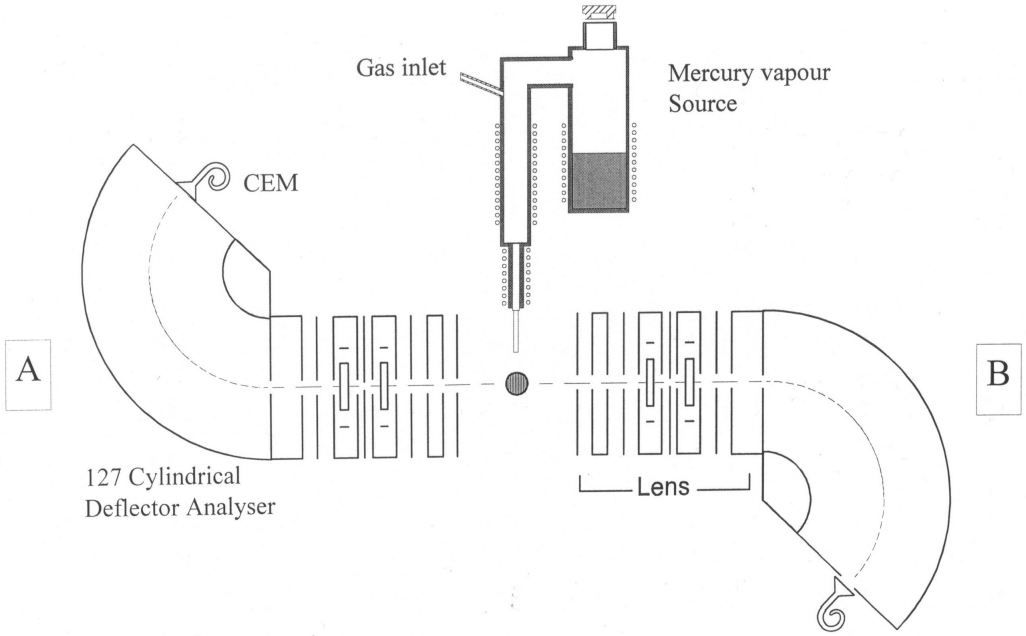

Figure 2 - Schematic of photoelectron spectrometer

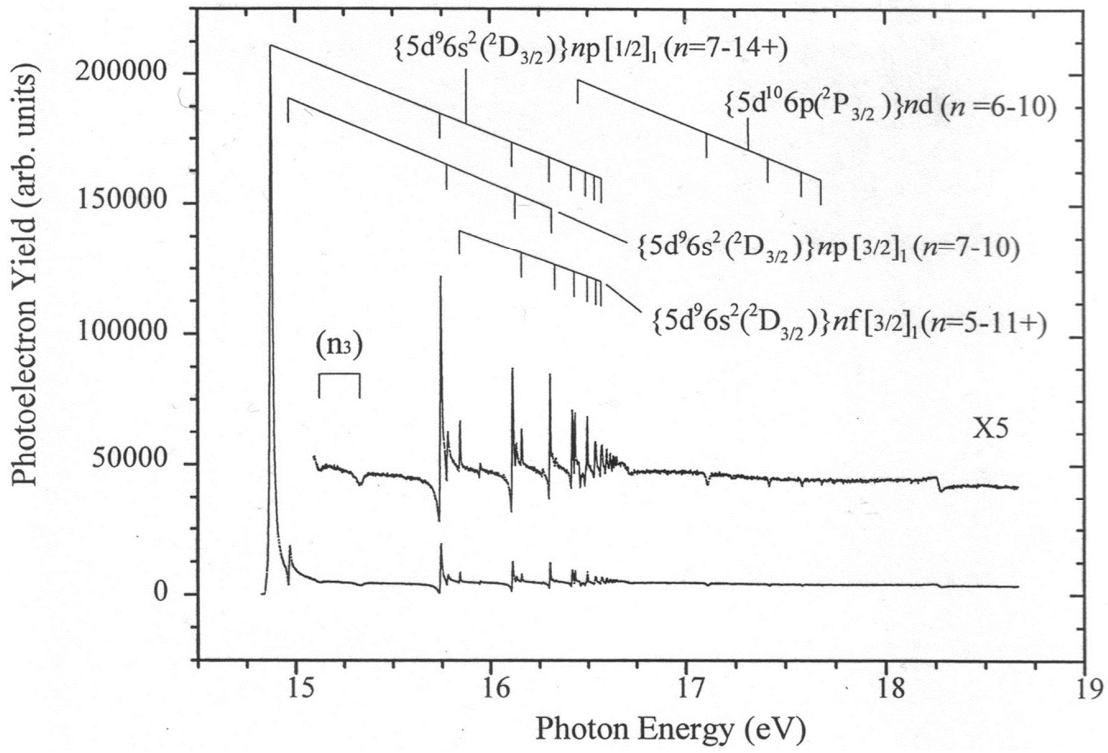

Figure 3 - CIS spectrum of the $^2D_{5/2}$ ionic state from the ionic threshold at 14.84eV to 18.65eV

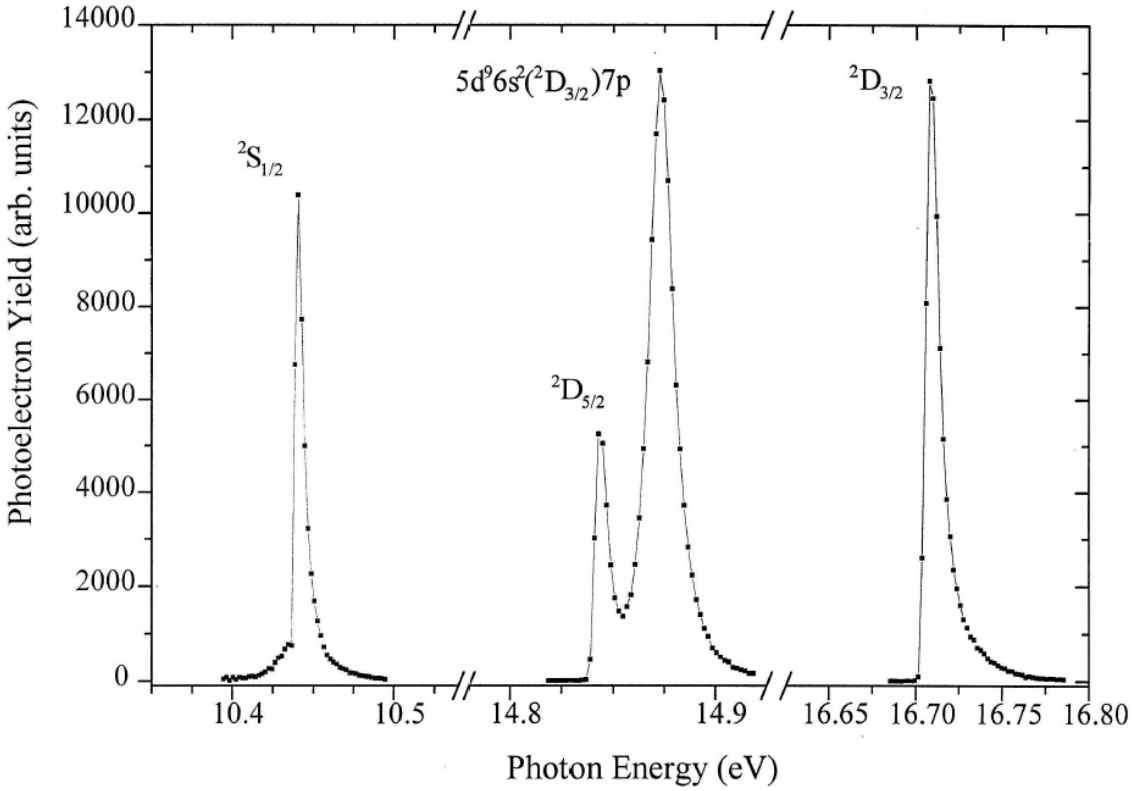

Figure 4 - TPES spectrum of lower lying single ionic states of mercury together with highly excited neutral state $\{5d^96s^2(^2D_{3/2})\}7p$.

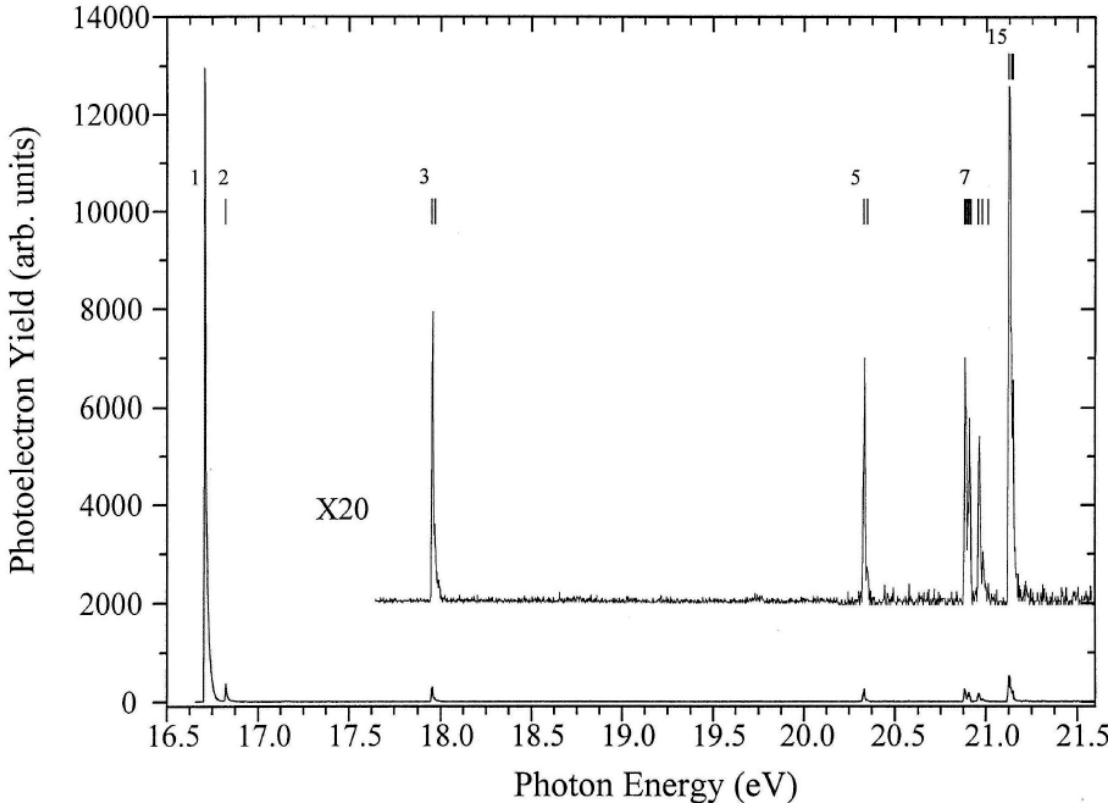

Figure 5 - TPES spectrum in the region of satellite states of Hg^+ (16.5 to 21.5 eV).

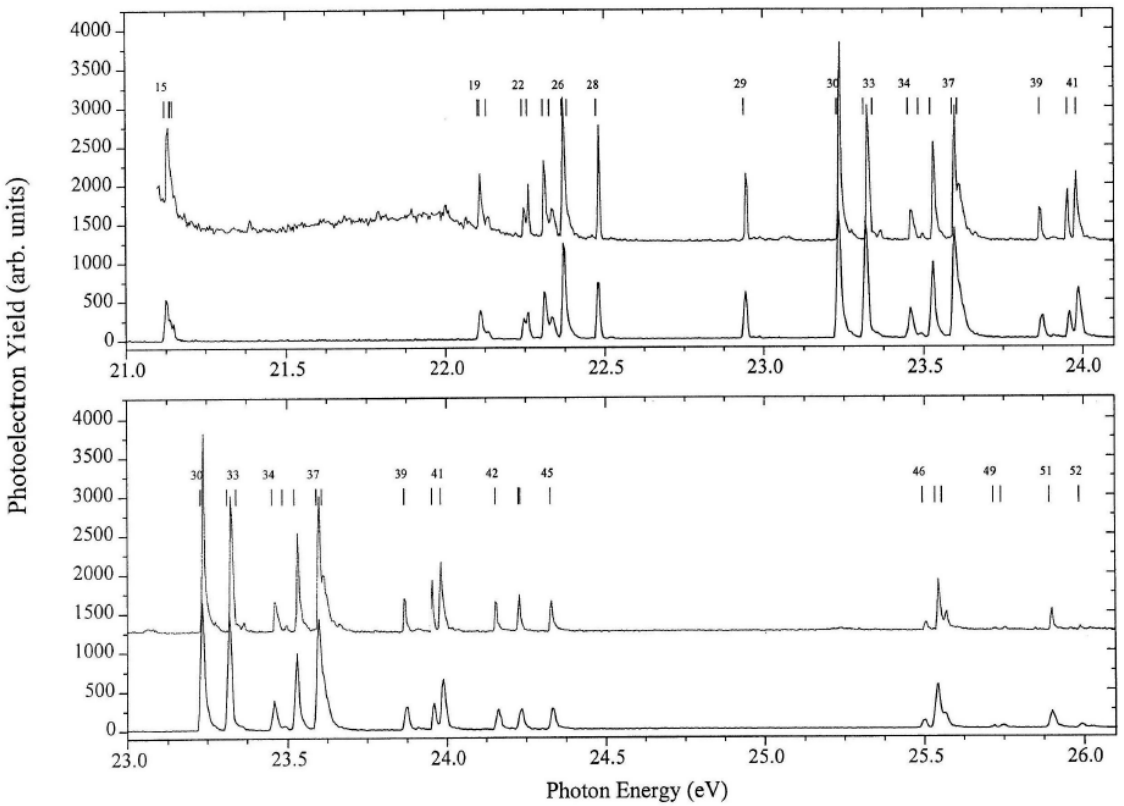

Figure 6- TPES spectrum in the region of satellite states of Hg^+ (21.0 to 26.1 eV). Also shown TPES spectrum obtained via second order light (top).

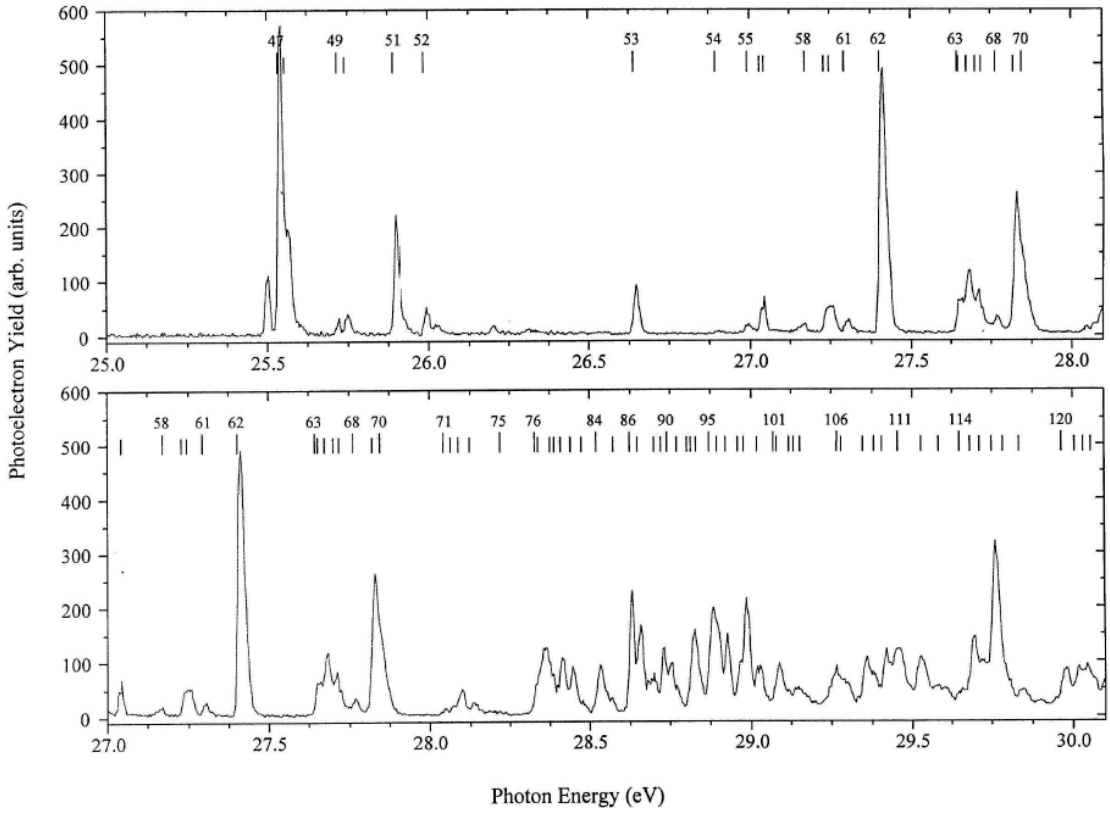

Figure 7 - TPES spectrum in the region of satellite states of Hg^+ (25.0 to 30.1 eV)

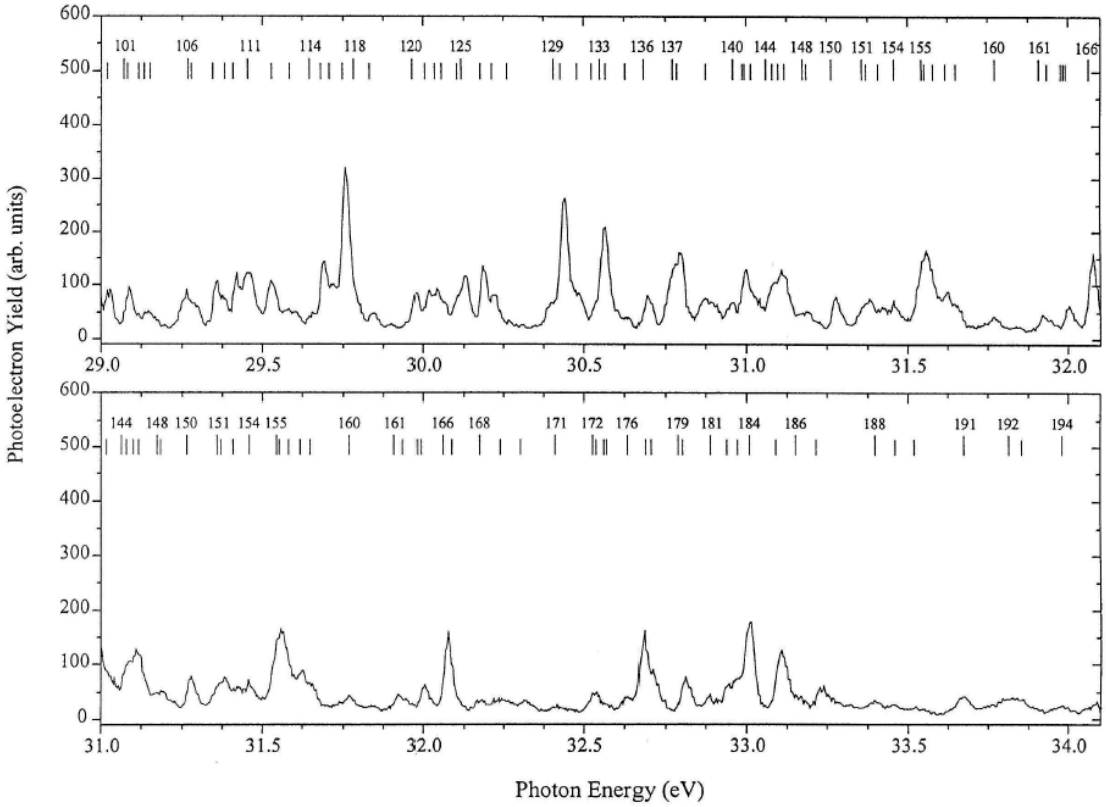

Figure 8 - TPES spectrum in the region of satellite states of Hg^+ (29.0 to 34.1 eV)

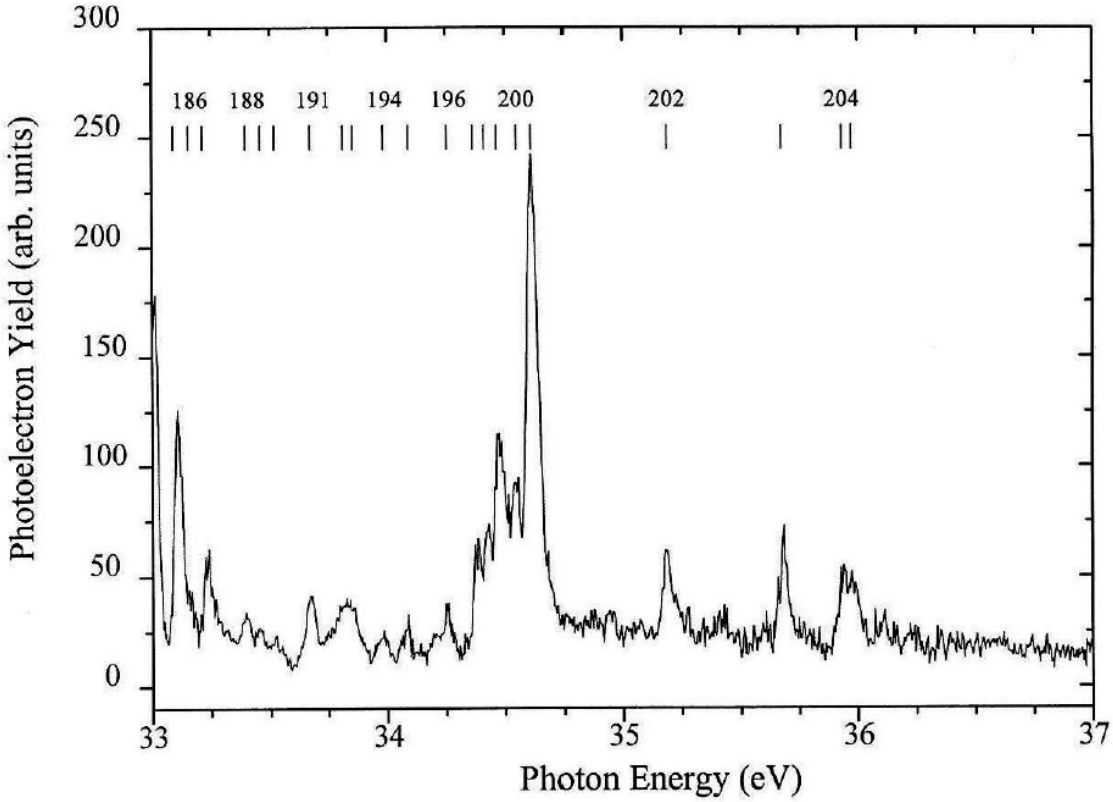

Figure 9 - TPES spectrum in the region of satellite states of Hg^+ (33.0 to 37.0 eV).

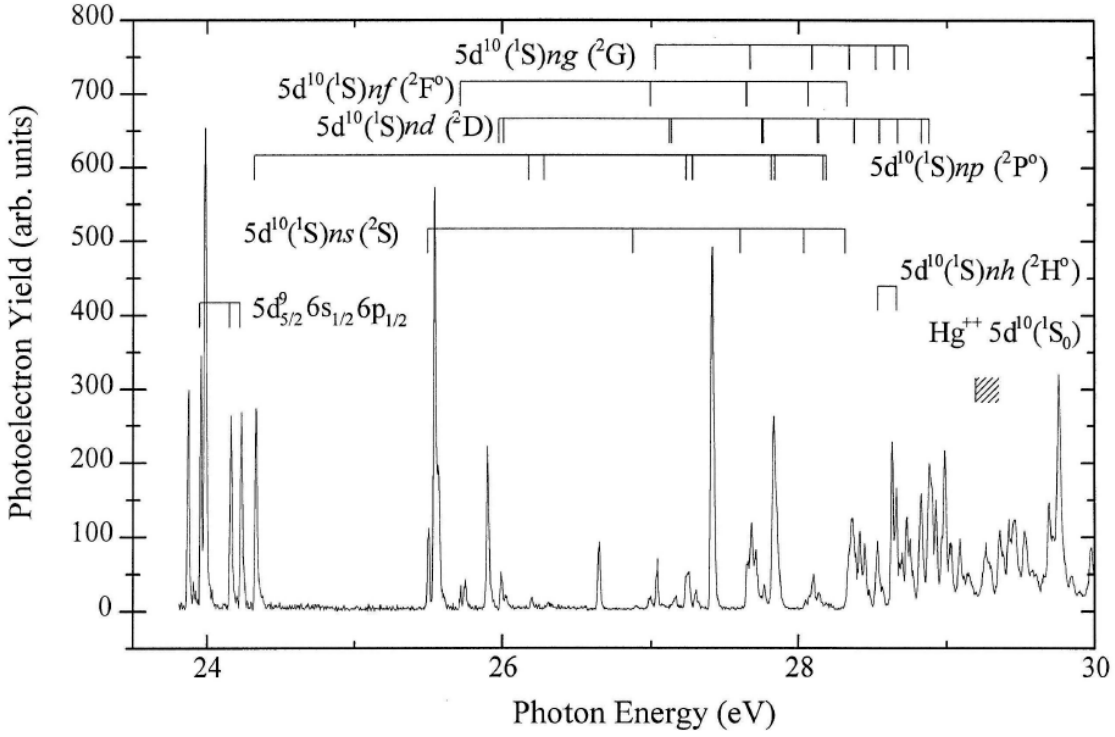

Figure 10 - TPES spectrum in the region of satellite states of Hg^+ below the $5d^{10}(^1S_0)$ double ionic threshold. Indicated are the $5d^{10}(^1S_0)$nl states identified and the $5d^9{}_{5/1}6s_{1/2}6p_{1/2}$ states in this energy region.

[1] Beutler, H. (1933) Z. Phys. **86** 710.
[2] Beutler, H. and Demeter, W. (1934) Z. Phys. **91** 218.
[3] Beutler, H. and Guggenheirmer, K. (1934) Z. Phys. **88** 25.
[4] Garten, W. R. S. and Connerade, J. P. (1969) Astrophys. J. **155** 667.
[5] Mansfield, M. W. D. (1973) Astrophys. J. **180** 1011.
[6] Learner, R. C. M and Morris, J. (1971) J. Phys. B: At. Mol. Phys. **4** 1236.
[7] Martin, W. C., Sugar, J. and Tech, J. L. (1972a) J. Opt. Soc. Am. **62**1488.
[8] Martin, W. C., Sugar, J. and Tech, J. L. (1972b) Phys. Rev. A. **6** 2022.
[9] Berkowitz , J., Dehmer, J. L., Kim, Y-K and Desclaux, J. P. (1974) J. Chem. Phys. **61** 2556.
[10] Shannon, S. P. and Codling K. (1978) J. Phys. B: At. Mol. Phys. **11** 1193.
[11] Walker, T. E. H. and Waber, J. T. (1974) J. Phys. B: At. Mol. Phys. **7** 674.
[12] Süzer S., Lee S. T. and Shirley D. A. (1976) Phys. Rev. A **13** 1842.
[13] Eland, J. H. D. and Feifel, R. (2004) J. Phys. Chem. A **108**, 9721.
[14] Toffoli, D., Stener, M. and Decleva, P. (2002) Phys. Rev. A **66**,012501.
[15] Zubek, M., Thompson, D. B., Bolognesi, P., Cooper, D. and King, G. C. (2005) J. Phys. B: At. Mol. Opt. Phys. **38** 1657.
[16] Baig, M. A. (2008) Eur. Phys. J. D 46, 437.
[17] Baer, T. and Guyon, P.-M. (1995), *An Historical Introduction to Threshold Photoionization* in High Resolution Laser Photoionization and Photoelectron Studies, Eds. Powis, I., Baer, T. and Ng, C.-Y., John Wiley & Sons, Chichester, England.
[18] King, G.C., Zubek, M., Rutter, P.M. and Read, F.H. (1987) J. Phys. E: Sci Instrum. **20** 440.
[19] Hall, R. I., Avaldi, L., Dawber, G., Zubek, M. and King, G. C. (1990) J. Phys. B: At. Mol. Phys. **23** 4469.
[20] Cvejanovic, S. and Read, F.H. (1974) J. Phys. B: At. Mol. Phys. **7** 1180.
[21] Moore, C. E. (1949) *Atomic Energy Levels*, National Standards Reference Data System USA Vol. 1.
[22] Smith, N. V. and Himpsel, F. J. (1983) *Handbook on Synchrotron Radiation*, Ed. Koch, E. E., Amsterdam, North-Holland, Vol. 1, 905.
[23] Price, S. D. and Eland, J. H. D. (1990) J. Phys. B: At. Mol. Phys. **23** 2269.